

# A Gas-Phase Investigation of Oxygen-Hydrogen Exchange Reaction of $O(^3P) + C_2H_5 \rightarrow H(^2S) + C_2H_4O^\dagger$

Su-Chan Jang, Min-Jin Park, and Jong-Ho Choi\*

Department of Chemistry, Research Institute for Natural Sciences, Korea University, Seoul 136-701, Korea

\*E-mail: jhc@korea.ac.kr

Received September 25, 2013, Accepted October 11, 2013

The gas-phase radical-radical reaction  $O(^3P) + C_2H_5$  (ethyl)  $\rightarrow H(^2S) + CH_3CHO$  (acetaldehyde) was investigated by applying a combination of vacuum-ultraviolet laser-induced fluorescence spectroscopy in a crossed beam configuration and *ab initio* calculations. The two radical reactants  $O(^3P)$  and  $C_2H_5$  were respectively produced by photolysis of  $NO_2$  and supersonic flash pyrolysis of the synthesized precursor azoethane. Doppler profile analysis of the nascent H-atom products in the Lyman- $\alpha$  region revealed that the average translational energy of the products and the average fraction of the total available energy released as translational energy were  $5.01 \pm 0.72$  kcal mol<sup>-1</sup> and 6.1%, respectively. The empirical data combined with CBS-QB3 level *ab initio* theory and statistical calculations demonstrated that the title exchange reaction is a major channel and proceeds *via* an addition-elimination mechanism through the formation of a short-lived, dynamical addition complex on the doublet potential energy surface. On the basis of systematic comparison with several exchange reactions of hydrocarbon radicals, the observed small kinetic energy release can be explained in terms of the loose transition state with a product-like geometry and a small reverse activation barrier along the reaction coordinate.

**Key Words :** Ethyl radicals, Oxygen-hydrogen exchange reaction, Crossed-beam apparatus, Doppler spectra, *Ab initio* calculations

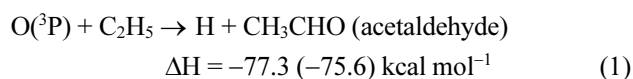
## Introduction

Preparation of short-lived radicals and investigation of their microscopic reaction mechanisms at the molecular level are considered to be extremely significant but unexplored aspects of chemical reaction dynamics. The gas-phase radical-radical reaction dynamics between ground-state atomic oxygen  $O(^3P)$  and hydrocarbon radicals is archetypal of this class of reactions. Despite the ubiquity and significance of elementary  $O(^3P) +$  hydrocarbon radical reactions in organic synthesis, combustion, plasma processes, and atmospheric and interstellar chemistry, studies of this class of reactions are quite limited relative to the plethora of studies on the reactions of  $O(^3P)$  with closed-shell hydrocarbon molecules amassed over several decades.<sup>1-3</sup> The lack of intimate mechanistic information on this important study is mainly due to the experimental difficulty in producing high concentrations of pure radicals and implementing reliable characterization methods. In conventional pyrolytic effusion sources, radicals inevitably undergo recombination and/or secondary dissociation due to the long residence time inside the hot tube after pyrolysis. In contrast, in the supersonic flash pyrolysis source developed by Chen, labile precursors entrained in a molecular beam experience a very short residence time inside a hot SiC tube, resulting in rapid thermal decomposition into clean, jet-cooled radical beams

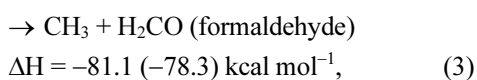
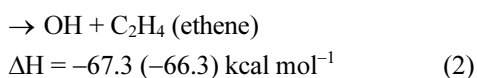
suitable for dynamical investigations in the gas phase.<sup>4</sup>

By adopting the supersonic flash pyrolysis source, a series of combined crossed-beam and theoretical studies of the prototypal oxidation reactions of both  $\pi$ -conjugated hydrocarbon radicals such as allyl ( $C_3H_5$ ), propargyl ( $C_3H_3$ ), vinyl ( $C_2H_3$ ), and saturated hydrocarbon radicals such as *t*-butyl (*t*- $C_4H_9$ ), ethyl ( $C_2H_5$ ), and *iso*-propyl (*i*- $C_3H_7$ ) have recently been executed in our laboratory.<sup>5-11</sup> The analyses of the energy distributions of the nascent reaction products have demonstrated extraordinary reactivity and mechanistic characteristics, which have not previously been observed in the reactions of  $O(^3P) +$  closed-shell hydrocarbon molecules.<sup>12,13</sup> Based on the authors' theoretical calculations, Leonori *et al.* also studied the oxidation reaction of allyl radicals using a universal crossed-beam apparatus.<sup>14</sup>

The present paper describes the first account of gas-phase oxygen-hydrogen exchange reaction dynamics of  $O(^3P)$  with  $C_2H_5$  undertaken in our laboratory. In addition to the primary significance in elementary reactive scattering processes, the title reaction is known as an essential pathway under lean fuel conditions. Supersonic flash pyrolysis of the synthesized precursor (azoethane,  $C_2H_5-N_2-C_2H_5$ ) was employed to generate the  $C_2H_5$  radicals, which may then react by the following pathways:



<sup>†</sup>This paper is to commemorate Professor Myung Soo Kim's honourable retirement.



where the reaction enthalpies were determined from *ab initio* calculation of the heats of formation and the experimental values are presented in parentheses for comparison.<sup>15</sup> In the previous kinetic experiments conducted by Gutman and coworkers, the second-order rate constant and the branching ratio of the three channels, (1)-(3), over the temperature range of 295-600 K were determined to be  $k = 2.2 \pm 0.4 \times 10^{-10} \text{ cm}^3 \text{ molecule}^{-1} \text{ s}^{-1}$  and  $k_1 : k_2 : k_3 = 0.40 \pm 0.04 : 0.23 \pm 0.07 : 0.32 \pm 0.07$ , respectively. The observed high  $k$  suggests that the radical-radical reaction proceeds through fast and irreversible mechanisms.<sup>16-21</sup> In contrast, nascent OH products with strongly non-statistical internal energy distributions were observed in the dynamics experiments performed by Leone and co-workers based on study of reaction (2) by applying FT-IR spectroscopy.<sup>22</sup> The present authors also examined the OH products in a crossed-beam study and identified two competing pathways, *i.e.*, the direct abstraction process (major) *vs.* the addition-complex-forming process (minor).<sup>9</sup> Trajectory calculations were also attempted by Harding and co-workers to obtain high-pressure recombination rate constants.<sup>23</sup> In addition, *ab initio* calculations have been performed by several theoretical groups, including the present authors, to examine various reaction channels of  $\text{O}(^3\text{P}) + \text{C}_2\text{H}_5$ .<sup>15,24,25</sup>

No gas-phase dynamics study of the reactive scattering process:  $\text{O}(^3\text{P}) + \text{C}_2\text{H}_5 \rightarrow \text{H}(^2\text{S}) + \text{C}_2\text{H}_4\text{O}$  has been reported to the best of our knowledge. Herein, the translational energy distributions of the nascent H-atom products are examined using tunable VUV-LIF spectroscopy in the Lyman- $\alpha$  region. With the aid of *ab initio* theory and statistical calculations, the reactivity and mechanistic characteristics of the title reaction at the molecular level are discussed on the basis of systematic comparison with several oxygen-hydrogen exchange reactions of hydrocarbon radicals.

### Experimental and *Ab initio* Calculations

The crossed-beam apparatus used in this study was made in-house and has been described in detail elsewhere.<sup>3,5-11</sup> In brief, a pulsed  $\text{O}(^3\text{P})$  radical beam was produced by irradiating 2 atm of He (ultra-high-purity helium: 99.999%) seeded with 12%  $\text{NO}_2$  (99.5%, MG Industries) with 30 mJ pulses from a 355 nm Nd:YAG laser beam (Continuum Surelite II-10) near the throat of the supersonic expansion. A second  $\text{C}_2\text{H}_5$  radical beam was prepared by supersonic flash pyrolysis of the precursor, azoethane ( $\text{C}_2\text{H}_5\text{-N=N-C}_2\text{H}_5$ ), synthesized using the method of Renaud and Leitch.<sup>26</sup> Due to the low dissociation energy of the C-N bond ( $43.5 \text{ kcal mol}^{-1}$ ), the azoethane seeded in He at 2 atm undergoes quantitative thermal decomposition to  $\text{C}_2\text{H}_5$  and  $\text{N}_2$  within the hot SiC (silicon carbide) tube, and expands supersonically into the

scattering chamber. Both radical beams were crossed at right angles under a single collision condition at the center of the scattering chamber.

The Doppler spectra of the nascent atomic hydrogen products were obtained by recording the fluorescence from the resonant  $^2\text{P} \leftarrow ^2\text{S}$  VUV Lyman- $\alpha$  electronic excitation centered at 121.6 nm. Here, the tunable, coherent VUV radiation was obtained from a tripling cell using a nonlinear process: the visible radiation at 729.6 nm generated from the Nd:YAG laser-pumped dye laser system was frequency-doubled in a BBO crystal, and the resulting UV laser beam was then tightly focused onto the tripling cell filled with a Kr/Ar rare-gas mixture, where the Lyman- $\alpha$  line was generated. After passing through the center of the two intersecting radical beams, the VUV radiation was directed into the photoionization cell (filled with 3% NO in He at 7 Torr), which was directly affixed to the scattering chamber. The  $\text{NO}^+$  (ionization energy of 9.26 eV) photocurrent signal was recorded to normalize the LIF signals of the atomic hydrogen products. The resulting fluorescence was collected by a PMT (Hamamatsu R1259) interfaced to the boxcar average (Stanford SR250) and the IMB-PC for display and analysis. The overall timing sequence of the pyrolysis, the photolysis, and probe beam laser was controlled with a pulse delay generator (Stanford DG535).<sup>27-29</sup>

We previously presented an in-depth theoretical investigation of the  $\text{O}(^3\text{P}) + \text{C}_2\text{H}_5$  reaction, and thus only a relevant account is presented herein.<sup>15</sup> *Ab initio* calculations were performed using the density functional method and the complete basis set (CBS) model of Gaussian 09 systems on an IMB PC and Compaq Workstation (XP-1000).<sup>30,31</sup> All geometries of local minima and transition states along the reaction coordinates were optimized at the hybrid density functional B3LYP level using the 6-311G(d,p) basis sets as the initial guesses. Subsequently, the CBS-QB3 level of theory was employed to perform calculations that are more reliable. It should be pointed out that several groups have also performed independent *ab initio* calculations on a few reaction pathways of  $\text{O}(^3\text{P}) + \text{C}_2\text{H}_5$  using Gaussian programs.<sup>32-36</sup> Compared to those results, however, the estimated heats of formation and reaction enthalpies for various species and pathways determined by the current protocol are in stronger agreement with the known experimental values within an accuracy of  $1.5 \text{ kcal mol}^{-1}$ .<sup>15</sup>

### Results

The Doppler-broadened spectral profiles of the atomic hydrogen product released under single-collision conditions are directly associated with the fraction of the total available energy partitioned into translational energy and provide important mechanistic information about the way in which the reactive scattering process occurs at the molecular level.

Figure 1 displays the typical Doppler spectra of the nascent H-atom products using the one-photon resonant  $^2\text{P} \leftarrow ^2\text{S}$  Lyman- $\alpha$  transition in the VUV region, centered at 121.6 nm, along with the corresponding Newton diagram.

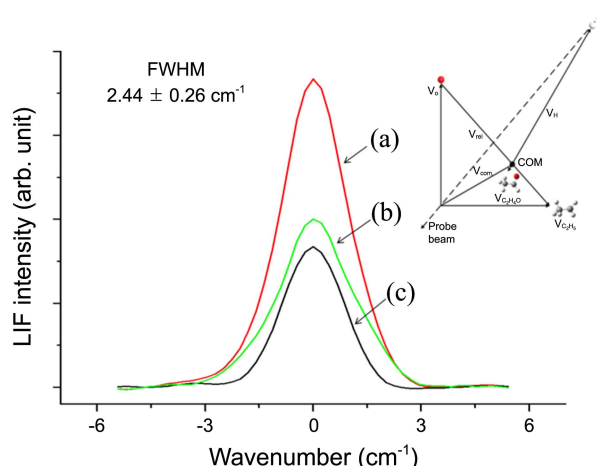


**Figure 1.** Typical VUV-LIF Doppler spectra of the H-atom products from the title reaction:  $\text{O}(^3\text{P}) + \text{C}_2\text{H}_5 \rightarrow \text{H}(^2\text{S}) + \text{C}_2\text{H}_4\text{O}$  (acetaldehyde) under a single collision condition. The interfering background (c: black line) was subtracted from the measured raw line profile (a: red line) to obtain the pure spectrum (b: green line) due solely to the title exchange reaction. The inset shows the Newton diagram of the title reaction.

The line profile (c: black line) in Figure 1 was acquired with the photolysis laser off to obtain the background spectrum through the direct Lyman- $\alpha$  photodissociation of  $\text{C}_2\text{H}_5$  radicals undergoing inelastic collisions with  $\text{NO}_2/\text{He}$ . The interfering background signals were subtracted directly from the raw profile (a: red line) to obtain a pure spectrum (b: green line) due solely to the title exchange reaction in Equation (1). The symmetric profile in Figure 1 was obtained after evaluating 11 individual Doppler spectra.

The Doppler-broadened spectra demonstrate that some fraction of the total available energy was released by conversion into the translational energy of the  $\text{H} + \text{CH}_3\text{CHO}$  products. Due to the high mass-partitioning factor [ $m(\text{H}) \ll m(\text{CH}_3\text{CHO})$ ], most of the released translational energy is expected to be directed to the H-atom products. In order to quantify the released energy, the average translational energy of the nascent H atoms  $\langle E_{\text{T}}^{\text{lab}}(\text{H}) \rangle$  in the laboratory frame was first evaluated from the spectra. Assuming a spatially isotropic velocity distribution in the laboratory frame,  $\langle v_x^2 \rangle = \langle v_y^2 \rangle = \langle v_z^2 \rangle$ ,  $\langle E_{\text{T}}^{\text{lab}}(\text{H}) \rangle$  can be calculated directly from the equation:  $\langle E_{\text{T}}^{\text{lab}}(\text{H}) \rangle = [3m(\text{H})/2] \langle v_z^2 \rangle$ . Here,  $v_z$  represents the velocity component of the absorbing H-atoms along the propagation direction of the probe beam in the scattering plane (see the Newton diagram in the inset of Fig. 1). The second momentum of the laboratory velocity distribution,  $\langle v_z^2 \rangle$ , can be estimated using the following Doppler-broadened Gaussian profile expression:<sup>37-40</sup>

$$\langle v_z^2 \rangle = c^2 (\Delta\nu_{\text{D}} / 2\nu_0)^2 / (2\ln 2),$$

where  $c$  is the speed of light,  $\nu_0$  is the central absorption frequency of the H atom at rest, and  $\Delta\nu_{\text{D}}$  is the full width at half maximum (FWHM). In this study, the averaged FWHM and  $\langle E_{\text{T}}^{\text{lab}}(\text{H}) \rangle$  values were determined to be  $2.44 \pm 0.26 \text{ cm}^{-1}$  and  $5.00 \pm 0.69 \text{ kcal mol}^{-1}$ , respectively.

Because the average kinetic energy in the laboratory frame,

$\langle E_{\text{T}}^{\text{lab}}(\text{O}-\text{C}_2\text{H}_5) \rangle$ , is given by the relation:

$$\langle E_{\text{T}}^{\text{lab}}(\text{O}-\text{C}_2\text{H}_5) \rangle = [m(\text{O}) \langle E_{\text{T}}^{\text{lab}}(\text{O}) \rangle + m(\text{C}_2\text{H}_5) \times \langle E_{\text{T}}^{\text{lab}}(\text{C}_2\text{H}_5) \rangle] / m(\text{C}_2\text{H}_5\text{O}),$$

the average translational energy of the  $\text{H} + \text{C}_2\text{H}_4\text{O}$  products in the center-of-mass (COM) frame,  $\langle E_{\text{T}}^{\text{com}} \rangle$ , can be estimated from  $\langle E_{\text{T}}^{\text{lab}}(\text{H}) \rangle$  and the expression:

$$\langle E_{\text{T}}^{\text{com}} \rangle = [m(\text{C}_2\text{H}_5\text{O})/m(\text{C}_2\text{H}_4\text{O})][\langle E_{\text{T}}^{\text{lab}}(\text{H}) \rangle - m(\text{H}) \langle E_{\text{T}}^{\text{lab}}(\text{O}-\text{C}_2\text{H}_5) \rangle / m(\text{C}_2\text{H}_5\text{O})].$$

The averaged  $\langle E_{\text{T}}^{\text{lab}}(\text{O}-\text{C}_2\text{H}_5) \rangle$  and  $\langle E_{\text{T}}^{\text{com}} \rangle$  values obtained herein were 5.97 and  $5.01 \pm 0.72 \text{ kcal mol}^{-1}$ , respectively. The average fraction,  $f_{\text{T}}$ , was eventually determined from the relation:  $f_{\text{T}} = \langle E_{\text{T}}^{\text{com}} \rangle / E_{\text{avl}}$ , where the total available energy,  $E_{\text{avl}}$ , is given by the equation:  $E_{\text{avl}} = E_{\text{com}} + E_{\text{int}}(\text{C}_2\text{H}_5) - \Delta H_{\text{rxn}}$ , where  $E_{\text{com}}$  is the COM collision energy of 5.2 kcal  $\text{mol}^{-1}$ ,  $E_{\text{int}}(\text{C}_2\text{H}_5)$  is the internal energy of the  $\text{C}_2\text{H}_5$  radical reactant, which is negligible ( $0.4 \text{ kcal mole}^{-1}$ ) in supersonic molecular beams, and  $\Delta H_{\text{rxn}}$  is the reaction enthalpy. The fraction for the title reaction was estimated to be *ca.* 6.1%.

## Discussion

**Microscopic Mechanism of the Oxygen-Hydrogen Reaction.** The comprehensive mechanistic information necessary to facilitate interpretation of the experimental data can be obtained from *ab initio* calculations. A complete and detailed description of all the pathways of the reaction  $\text{O}(^3\text{P}) + \text{C}_2\text{H}_5$  was presented in our previous paper,<sup>15</sup> and here we focus on reaction pathway (1) where atomic hydrogen is released. Figure 2 shows a schematic pathway of the title reaction along with the geometries of the intermediate and the transition state. The overall pathway is a conventional addition-elimination process. As atomic oxygen attacks  $\text{C}_2\text{H}_5$  along the entrance reaction coordinate, the strong, long-range attractive interaction between the two reactive radicals leads to an energized  $\text{C}_2\text{H}_5\text{O}$  intermediate, denoted as eINT1 in Figure 2.

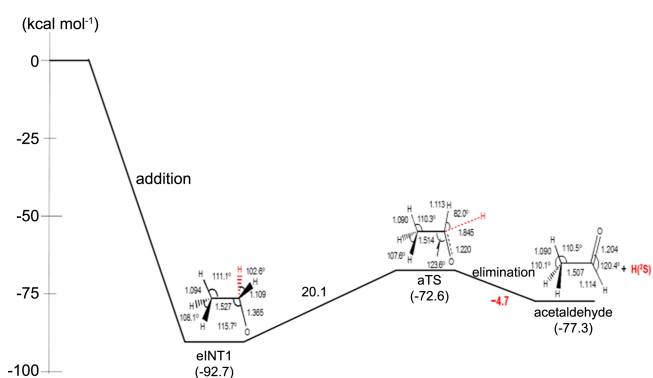


**Figure 2.** Schematic pathway of the title reaction:  $\text{O}(^3\text{P}) + \text{C}_2\text{H}_5 \rightarrow \text{H}(^2\text{S}) + \text{CH}_3\text{CHO}$  (acetaldehyde) with the optimized geometries computed at the CBS-QB3 level of theory. The values denote the zero-point-energy-corrected total energies relative to  $\text{O}(^3\text{P}) + \text{C}_2\text{H}_5$ , and the values above the arrows denote the forward activation barrier (positive) and released exit-channel energy (negative) in  $\text{kcal mol}^{-1}$ .

The barrierless initiation is typical of reactions between two open-shell species, and the overall addition process was estimated to be highly exothermic ( $-92.7$  kcal mol $^{-1}$ ) with respect to the reactants O + C $_2$ H $_5$ . Due to very high internal energy, subsequent isomerization and/or decomposition of the energized eINT1, leading to various products, may preclude redissociation into reactant radicals. As shown in Figure 2, direct cleavage of the C(1)-H bond of eINT1 through the transition state aTS1 with a barrier height of 20.1 kcal mol $^{-1}$  results in the formation of acetaldehyde (CH $_3$ CHO) + H in the title reaction (1) ( $\Delta H = -77.3$  kcal mol $^{-1}$ ). Although the activation barrier appears to be considerable, the value nevertheless lies well within the available energy of the energized intermediate. After considering the barrier height and reaction exothermicity along the reaction coordinate, the title reaction is, in fact, predicted to be a major channel, which is consistent with the gas-phase kinetic experiments.<sup>5-11</sup>

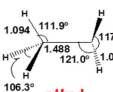
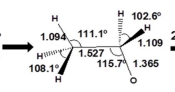
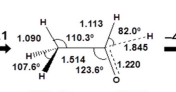
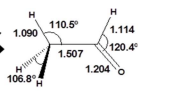
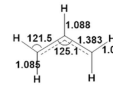
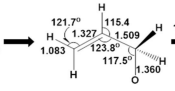
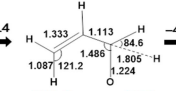
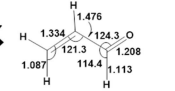
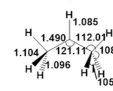
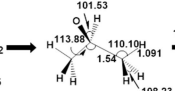
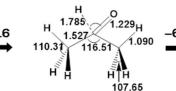
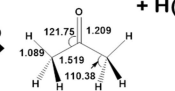
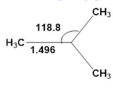
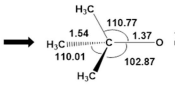
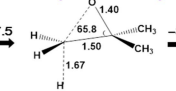
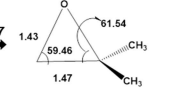
**Statistical Analyses and Reaction Dynamics.** The partitioning of the energy into the H products and the microscopic kinetic rate constants were derived using the aforementioned *ab initio* calculations. The Levine-Bernstein *prior* method and microcanonical RRKM (Rice-Ramsperger-Kassel-Marcus) theory are two simple but very efficient statistical approaches to obtain quantitative information.<sup>41-45</sup> Both schemes are based upon the assumption that energized intermediates, such as eINT1 in Figure 2, are sufficiently long-lived to allow the entire available energy to be equally partitioned among all the degrees of freedom prior to unimolecular decomposition, and that the product state distribution is determined wholly by the available volume in phase space of the two fragment products. The Levine-Bernstein *prior* fraction was predicted to be 13.0%, which is larger than the experimental  $f_T$  of 6.1%. For the energy-specific RRKM rate constant,  $k_f(E_{\text{avl}})$ , assuming a full expansion of the super-

sonic radical beams,  $k_f(E_{\text{avl}} = 97.9$  kcal mol $^{-1}$ ) was estimated to be  $5.75 \times 10^{12}$  s $^{-1}$  under the crossed-beam conditions. The high value of  $k_f(E_{\text{avl}})$  is attributed mainly to overcoming the aTS transition state with a low barrier height of 20.1 kcal mol $^{-1}$ .

The distinctive disagreement between the  $f_T$  values of the Levine-Bernstein *prior* estimate and the crossed-beam experiment suggests that the H-atom release process has a clear dynamical bias derived from short-lived addition complexes rather than long-lived, statistical complexes. Most of the available energy is released through the channel of internal excitation of the counterpart product CH $_3$ CHO (acetaldehyde). The observed dynamics can be rationalized based on comparison with other H-atom release reactions studied by the authors. Figure 3 outlines the comparative energy profiles of four oxygen-hydrogen exchange reactions of *t*-butyl, *iso*-propyl, allyl, and ethyl radicals on the spin-orbit state-averaged energy surfaces, and Table 1 summarizes the corresponding estimates of  $\Delta H$ ,  $\Delta v_D$ ,  $\langle E_T^{\text{com}} \rangle$ , and  $f_T$  for comparison.

As revealed in the simplified profiles, the H-atom release dynamics associated with the non-statistical  $f_T$  values is strongly correlated with *both* the structural characteristics of the transition state and the magnitude of the reverse activation barrier. The transition state can be divided into three different classes: *tight*, *medium*, and *loose*. In the case of the tight transition state, due to the shorter C-H bond on a repulsive state, a stronger instantaneous force is exerted during unimolecular decomposition. In addition, after passing through the transition-state region, the higher reverse barrier along the reaction coordinates causes the reaction products to move rapidly down the repulsive wall with considerable energy, with lower probability of exchanging the available energy through intramolecular energy redistribution. Consequently, the tight transition-state geometry, having a large

**Table 1.** Comparative schematic pathways of four radical-radical oxidation reactions with the geometries of the intermediates and transition states, and estimates of  $\Delta H$ ,  $\Delta v_D$ ,  $\langle E_T^{\text{com}} \rangle$  and  $f_T$ . The values above the arrows denote the forward activation barriers (positive) and released exit-channel energies (negative) in kcal mol $^{-1}$

Reactants	INT	TS	Products	$\Delta H$ (kcal mol $^{-1}$ )	$\Delta v_D$ (cm $^{-1}$ )	$\langle E_T^{\text{com}} \rangle$ (kcal mol $^{-1}$ )	$f_T$
 ethyl		 aTS (Loose TS)		-77.3	2.44	5.01	0.061
 allyl		 acTS (Loose TS)		-63.9	2.13	3.83	0.054
O( $^3P$ ) +  <i>iso</i> -propyl		 atTS (Medium TS)	 + H( $^2S$ )	-82.2	6.15	33.3	0.38
 <i>t</i> -butyl		 iTS (Tight TS)		-54.8	7.64	50.1	0.83

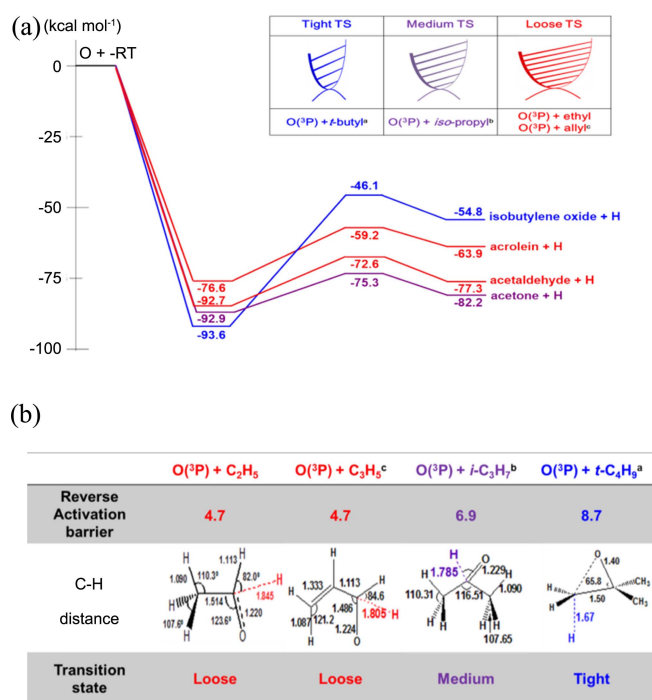


**Figure 3.** (a) Comparative schematic pathways of four different reactions; geometries of the transition states, estimates of reverse activation barriers, and C-H distances are shown. (b) A comparative diagram of four different transition states leading to the H-atom products. The observed  $f_T$  values are strongly correlated with the geometric features of the transition states and the magnitude of the reverse activation barriers along the reaction coordinates. <sup>a</sup>reference 8, <sup>b</sup>reference 5, <sup>c</sup>reference 6.

exit-channel energy, is expected to lead to the formation of ejected H products with a higher  $f_T$  of translational energy at the molecular level, as illustrated by the  $O + t$ -butyl reaction in Table 1.<sup>8</sup> On the other hand, in the case of the  $O +$  allyl reaction, the situation is totally reversed due to the longer C-H bond length in the loose, product-like transition state and the small exit-channel energy, resulting in the low  $f_T$  value.<sup>6</sup> In the case of the medium transition state, the observed  $f_T$  value can be attributed to the medium C-H bond length and reverse activation barrier, as shown in the  $O + iso$ -propyl reaction.<sup>5</sup> In the case of the title  $O(^3P) +$  ethyl reaction, the observed small  $f_T$  value can be attributed to both the long C-H bond length (1.85 Å) and the small reverse activation barrier (4.7 kcal mol<sup>-1</sup>), which corresponds to occurrence of the dynamics in the loose transition state.

As revealed in this comprehensive study, the unique H-atom release dynamics in the oxidation reactions of hydrocarbon radical systems can be effectively probed by applying a combined crossed-beam and *ab initio* investigation. The observed non-statistical, kinetic energy release suggests that the radical-radical reaction dynamics in the gas phase is quite sensitive to the detailed profile of the potential energy surface, particularly in the region of the transition state.

### Conclusion

The H-atom products from the radical-radical reaction:

$O(^3P) + C_2H_5 \rightarrow H(^2S) + CH_3CHO$  were examined using combined crossed-beam and *ab initio* investigations. The title oxygen-hydrogen exchange reaction was found to be a major pathway and proceeded *via* an addition-elimination mechanism involving the formation of a dynamical addition complex on the doublet potential energy surface. Based on systematic comparison with several exchange reactions of hydrocarbon radicals, the observed small kinetic energy release can be rationalized in terms of the loose, product-like transition state and the internally excited counterpart product.

As established in this study, the gas-phase reaction dynamics presented herein is a step forward in understanding elementary radical-radical reactive scattering processes. Extensive crossed-beam investigations combined with theoretical calculations on the oxidation reactions of various hydrocarbon radicals, including aromatic transient species such as benzyl and phenyl moieties, are currently being conducted. It is the hope of the authors that this gas-phase study will provide detailed mechanistic insights into the extremely reactive radical-radical reactions at the molecular level.

**Acknowledgments.** This work was supported by the Korea University, LG Yonam Foundation, and Basic Science Research Program through the National Research Foundation of Korea (NRF) funded by the Ministry of Education (NRF20100020209).

### References

- Levine, R. D.; Bernstein, R. B. *Molecular Reaction Dynamics and Chemical Reactivity*; Oxford University Press: New York, U.S.A., 1987.
- Casavecchia, P.; Leonori, F.; Balucani, N.; Petrucci, R.; Capozza, G.; Segoloni, E. *Phys. Chem. Chem. Phys.* **2009**, *11*, 46-65.
- Choi, J. H. *Int. Rev. Phys. Chem.* **2006**, *25*, 613-653.
- Kohn, D. W.; Clauberg, H.; Chen, P. *Rev. Sci. Instrum.* **1992**, *63*, 4003-4005.
- Park, M. J.; Jang, S. C.; Choi, J. H. *J. Phys. Chem. A* **2013**, *117*, 12020-12025.
- Joo, S. K.; Kwon, L. K.; Lee, H.; Choi, J. H. *J. Chem. Phys.* **2004**, *120*, 7976-7982.
- Kwon, L.; Nam, M. J.; Youn, S. E.; Joo, S. K.; Lee, H.; Choi, J. H. *J. Chem. Phys.* **2006**, *124*, 204320-1~7.
- Youn, S. E.; Ok, Y. H.; Choi, J. H. *ChemPhysChem* **2008**, *9*, 1099-1103.
- Park, Y. P.; Kang, K. W.; Jung, S. H.; Choi, J. H. *Phys. Chem. Chem. Phys.* **2010**, *12*, 7098-7107.
- Kang, K. W.; Park, M. J.; Choi, J. H. *Phys. Chem. Chem. Phys.* **2011**, *13*, 8122-8126.
- Park, M. J.; Jang, S. C.; Choi, J. H. *J. Chem. Phys.* **2012**, *137*, 204311-1~10.
- Kleiner, K.; Luntz, A. C. *J. Chem. Phys.* **1982**, *77*, 3533-3536.
- Andresen, P.; Luntz, A. C. *J. Chem. Phys.* **1980**, *72*, 5842-5850.
- Leonori, F.; Balucani, N.; Capozza, G.; Segoloni, E.; Stranges, D.; Casavecchia, P. *Phys. Chem. Chem. Phys.* **2007**, *9*, 1307-1311.
- Jung, S. H.; Park, Y. P.; Kang, K. W.; Park, M. J.; Choi, J. H. *Theor. Chem. Acc.* **2011**, *129*, 105-118.
- Baulch, D. L.; Bowman, C. T.; Cobos, C. J.; Cox, R. A.; Just, T.; Kerr, J. A.; Pilling, M. J.; Stocker, D.; Troe, J.; Tsang, W.; Walker, R. W.; Warnatz, J. *J. Phys. Chem. Ref. Data* **2005**, *34*, 757-1397.
- Slage, I. R.; Sarzynski, D.; Gutman, D.; Miller, J. A.; Melius, C.



- F. J. Chem. Soc. Faraday Trans.* **1988**, *84*, 491-503.
18. Hoyermann, K.; Olzmann, M.; Seeba, J.; Viskolcz, B. *J. Phys. Chem. A* **1999**, *103*, 5692-5698.
19. Hack, W.; Hoyermann, K.; Olzmann, M.; Zeuch, T. *Proc. Combust. Inst.* **2002**, *29*, 1247-1255.
20. Linder, J.; Loomis, R. A.; Klaassem, J. J.; Leone, S. R. *J. Chem. Phys.* **1998**, *108*, 1944-1952.
21. Herron, J. T. *J. Phys. Chem. Ref. Data* **1988**, *17*, 967-1026.
22. Reid, J. P.; Marcy, T. P.; Kuehn, S.; Leone, S. R. *J. Chem. Phys.* **2000**, *113*, 4572-4580.
23. Harding, L. B.; Klippenstein, S. J.; Georgievskii, Y. *Proc. Combust. Inst.* **2005**, *30*, 985-993.
24. Gupta, A.; Singh, R. P.; Singh, V. B.; Mishra, B. K.; Amurthy, N. S. *J. Chem. Sci.* **2007**, *119*, 457-465.
25. Yong, Y.; Weijin, Z.; Xiaoming, G.; Shixin, P.; Jie, S.; Wei, H.; Jun, Q. *Chin. J. Chem. Phys.* **2005**, *18*, 515-521.
26. Renaud, R.; Leitch, L. C. *Can. J. Chem.* **1954**, *32*, 545-549.
27. Hilber, G.; Lago, A.; Wallenstein, R. *J. Opt. Soc. Am. B* **1987**, *4*, 1753-1764.
28. Marangos, J. P.; Shen, N.; Ma, H.; Hutchinson, M. H. R.; Connerade, J. P. *J. Opt. Soc. Am. B* **1990**, *7*, 1254-1259.
29. Tonokura, K.; Murasaki, T.; Koshi, M. *Chem. Phys. Lett.* **2000**, *319*, 507-511.
30. Frisch, M. J.; Trucks, G. W.; Schlegel, H. B.; Scuseria, G. E.; Robb, M. A.; Cheeseman, J. R.; Scalmani, G.; Barone, V.; Mennucci, B.; Petersson, G. A.; Nakatsuji, H.; Caricato, M.; Li, X.; Hratchian, H. P.; Izmaylov, A. F.; Bloino, J.; Zheng, G.; Sonnenberg, J. L.; Hada, M.; Ehara, M.; Toyota, K.; Fukuda, R.; Hasegawa, J.; Ishida, M.; Nakajima, T.; Honda, Y.; Kitao, O.; Nakai, H.; Vreven, T.; Montgomery, J. A., Jr.; Peralta, J. E.; Ogliaro, F.; Bearpark, M.; Heyd, J. J.; Brothers, E.; Kudin, K. N.; Staroverov, V. N.; Kobayashi, R.; Normand, J.; Raghavachari, K.; Rendell, A.; Burant, J. C.; Iyengar, S. S.; Tomasi, J.; Cossi, M.; Rega, N.; Millam, N. J.; Klene, M.; Knox, J. E.; Cross, J. B.; Bakken, V.; Adamo, C.; Jaramillo, J.; Gomperts, R.; Stratmann, R. E.; Yazyev, O.; Austin, A. J.; Cammi, R.; Pomelli, C.; Ochterski, J. W.; Martin, R. L.; Morokuma, K.; Zakrzewski, V. G.; Voth, G. A.; Salvador, P.; Dannenberg, J. J.; Dapprich, S.; Daniels, A. D.; Farkas, Ö.; Foresman, J. B.; Ortiz, J. V.; Cioslowski, J.; Fox, D. J. *Gaussian 09*, revision A.1.; Gaussian, Inc.: Wallingford, 2009.
31. Becke, A. D. *J. Chem. Phys.* **1992**, *96*, 2155-2160.
32. Becke, A. D. *J. Chem. Phys.* **1993**, *98*, 1372-1377.
33. Becke, A. D. *J. Chem. Phys.* **1993**, *98*, 5648-5652.
34. Curtiss, L. A.; Raghavachari, K.; Redfern, P. C.; Pople, J. A. *J. Chem. Phys.* **1997**, *106*, 1063-1079.
35. Lee, C.; Yang, W.; Parr, R. G. *Phys. Rev. B* **1988**, *37*, 785-789.
36. Baker, J.; Muir, M.; Andzelm, J. *J. Chem. Phys.* **1995**, *102*, 2063-2079.
37. Demtroder, W. *Laser Spectroscopy*; Springer-Verlag: Berlin Heidelberg, German, 1991.
38. Matsumi, Y.; Shafer, N.; Tonokura, K.; Kawasaki, M. *J. Chem. Phys.* **1991**, *95*, 4972-4976.
39. Matsumi, Y.; Tonokura, K.; Kawasaki, M. *J. Phys. Chem.* **1992**, *96*, 10622-10626.
40. Brownsword, R. A.; Hilenkamp, M.; Laurent, T.; Vatsa, R. K.; Volpp, H.-R. *Chem. Phys. Lett.* **1996**, *259*, 375-380.
41. Baer, T.; Hase, W. L. *Unimolecular Reaction Dynamics*; Oxford University Press: New York, U.S.A., 1996.
42. Holbrook, K. A.; Pilling, M. J.; Robertson, S. H. *Unimolecular Reactions*; Wiley & Sons: New York, U.S.A., 1996.
43. Wang, B.; Hou, H.; Gu, Y. *Chem. Phys. Lett.* **1999**, *304*, 278-284.
44. Huang, X.; Xing, G.; Bersohn, R. *J. Chem. Phys.* **1994**, *101*, 5818-5823.
45. Berman, M. R.; Lin, M. C. *J. Phys. Chem.* **1983**, *87*, 3933-3942.
-